Nano Energy 86 (2021) 106077

Contents lists available at ScienceDirect

Nano Energy

journal homepage: http://www.elsevier.com/locate/nanoen

Full paper

MXene enhanced self-powered alternating current electroluminescence devices for patterned flexible displays

Junlu Sun [a,b,1], Yu Chang [a,1], Lin Dong [a,*], Kuikui Zhang [a], Qilin Hua [b,c], Jinhao Zang [a], Qiushuo Chen [b], Yuanyuan Shang [a], Caofeng Pan [b,c], Chongxin Shan [a,*]

[a] Henan Key Laboratory of Diamond Optoelectronic Materials and Devices, Key Laboratory of Materials Physics, Ministry of Education, and School of Physics and Microelectronics, Zhengzhou University, 450001 China

[b] CAS Center for Excellence in Nanoscience, Beijing Key Laboratory of Micro-nano Energy and Sensor, Beijing Institute of Nanoenergy and Nanosystems, Chinese Academy of Sciences, Beijing 100083, China

[c] School of Nanoscience and Technology, University of Chinese Academy of Sciences, Beijing 100049, China

ARTICLE INFO

Keywords:
MXene
Self-powered
ACEL
Patterned display

ABSTRACT

Patterned displays with self-powered features have been crucial for event-driven information communication and exchange in the Internet of things (IoT) applications. Here, we present a MXene enhanced alternating current electroluminescence (ACEL) device array integrated with the triboelectric nanogenerator (TENG) as the self-powered patterned display. The ACEL device is intrinsically transparent and stretchable. And its emission intensity can be enhanced by 500% through filling 0.25 wt% MXene in the polymer matrix of emission layer, in accordance with the finite element analysis simulation of the electric field strength with various MXene loading. Finally, a patterned ACEL device is constructed and powered with a simple TENG for patterned display. This self-powered patterned ACEL display has considerable potential for applications of human-healthcare monitoring, information-security communication, and human-machine interface in IoT.

1. Introduction

Electroluminescence (EL), a phenomenon of light generation derived from an electric field, has been developed and utilized as vital part of illumination and displays in the plentiful fields including health-information monitoring [1–4], information-security communication [5–8], and human-machine interfaces [9,10]. Commonly, EL devices are classified into two categories: light-emitting diode (LED) and alternating current electroluminescence devices (ACEL). LED devices, such as organic LEDs [11–13], quantum dot LEDs [14–16], and p/n-junction LEDs [17–19], are driven at a low bias to cause the radiative recombination of electrons and holes; whereas for ACEL devices, a much higher electrical field intensity is usually necessary to induce the inelastic collision of luminescent center with high-energy electrons [20,21]. ACEL devices have attracted great attentions in the field of flexible electrons due to the uniformity of light emission, excellent contrast, high brightness, and extremely long working expectancy [22,23], however, the inevitable high driven voltage limits their application in human–machine interactions, artificial electronic skins, and smart wearable equipment in IoT.

Recently, self-powered devices/systems driven by triboelectric nanogenerators (TENGs) have attracted widespread concerns. Originating from the Maxwell's displacement current, TENG is first invented by Wang's group [24,25], which provided an appropriate strategy to harvest randomly distributed or irregular mechanical energy (such as winds [26], rain drops [27,28], human-body movements [29–32], ocean waves [33], and acoustic waves [34], etc.) into electric energy. Due to the inherent high output voltage of TENG, it is convenient to build high electric field and illuminate the ACEL devices. Hence, the self-powered ACEL system could be achieved by integrating with TENGs. Nevertheless, higher brightness and lower driving voltage is also vital for applications of ACEL devices in wearable and self-powered communication in IoT, whereas very rare work have been conducted in this regard.

Here, we introduce MXene into the emission layer to enhance the performance of self-powered ACEL devices. As a new class of two-dimensional (2D) materials consisting of transition metal and carbides/nitrides, MXene possesses outstanding electrochemical and thermoelectric properties [35–37]. Especially, MXenes have been utilized as

* Corresponding authors.
E-mail addresses: ldong@zzu.edu.cn (L. Dong), cxshan@zzu.edu.cn (C. Shan).
[1] These authors contributed equally to this work.

https://doi.org/10.1016/j.nanoen.2021.106077
Received 16 February 2021; Received in revised form 2 April 2021; Accepted 12 April 2021
Available online 19 April 2021

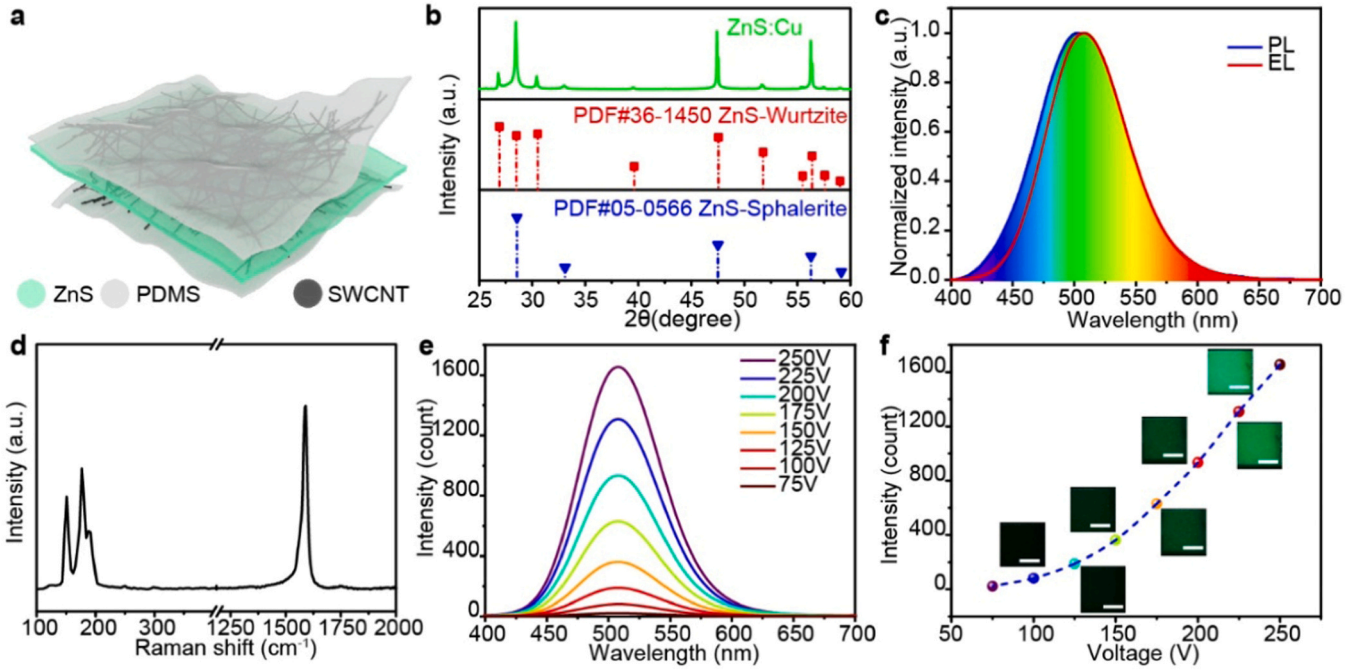

Fig. 1. Structure and characteristics of ACEL device. (a) The schematic illustration of ACEL device, consisting of two SWCNTs transparent electrodes and an emissive layer of ZnS:Cu. (b and c) X-ray diffraction patterns, PL, and EL spectrum of ZnS:Cu. d) Raman spectrum of SWCNTs. (e and f) EL spectra and the integrated intensity of ACEL device under various voltage, the corresponding photographs are shown in the inset. Scale bar: 5 mm.

fillers to significantly improve the dielectric constant of polymer matrix [38–40]. In our work, the relative permittivity of polymer matrix (polydimethylsiloxane, PDMS) is considerably enhanced with various MXene loadings. Hence, the brightness of the ACEL is also improved by 500% by loading 0.25 wt% MXene in the emission layer. A contact-mode TENG, with Cu as the positive charge collector and PTFE as the negative charge collector, is integrated with the ACEL to construct a self-powered ACEL system. The flexible patterned ACEL-TENG arrays are highly transparent, and would provide a powerful platform for self-power communication in IoT.

2. Experimental

2.1. Preparation of MXene

Firstly, 0.5 g Ti_3AlC_2 was etched by 0.8 g LiF and 10 mL concentrated HCl for 24 h. The resultants were purified by centrifugation with de-ion water for four times. Then the obtained multilayer Ti_3C_2 was dispersed in 40 mL water in a flask with ultrasound under N_2 atmosphere for 1 h. The Ti_3C_2 nanosheets were finally obtained.

2.2. Synthesis of SWCNTs

SWCNTs were synthesized through a chemical vapor deposition with catalyst in a horizontal tube at 1160 °C.as described in our previous work [41]. The carbon source (xylene) and catalyst (ferrocene) were carried by Ar mixed with 20% H_2 to the high temperature zone.

2.3. Fabrication of ACEL devices

The ACEL device consisted of two transparent SWCNTs electrodes and emissive ZnS:Cu layer. Firstly, the PDMS (SYL-GARD184, Dow Corning) main agent and curing agent (10:1 by weight) were mixed and transferred to a vacuum oven to exhaust bubbles. The obtained transparent PDMS solution was spin-coated onto glass substrate at 500 rpm, cured at 70 ℃ for 30 min, and then peeled off from the substrate. Secondly, the electrodes were fabricated by transferring synthesized SWCNTs on the PDMS film. The emissive layer was prepared by blending phosphor (ZnS:Cu) in PDMS matrix with a weight ratio of 20%. For MXene enhanced ACEL devices, MXene was added in the emissive layer with different weight ratio (0.00%, 0.25%, 0.50%, 0.75%, and 1.00%). Finally, two electrodes and emissive layer were stacked together to construct the ACEL device.

2.4. Preparation of self-powered ACEL device

A contact-separation mode TENG was fabricated based on two tribo-layers and two charge collector electrodes. The Polytetrafluoroethylene (PTFE) pretreated with oxygen plasma was used as negative tribo-layer. The negative charge collector was obtained by sputtering a layer of copper on the supporting substrate Kapton film. The corresponding positive tribo-layer and charge collector was a piece of copper foils adhered on 3 M foam tape, which serves as a buffer cushion. So, the ACEL device could be driven by a contact-separation modeled TENG through converting mechanical energy to electricity.

2.5. Characterization and measurements

The morphologies of MXene and the cross-section view of ACEL were measured by field-emission scanning electron microscopy (SU8020, Hitachi). The TEM image and SAED were collected through a JEM-TEM-2100F (JEOL). The crystal structure of ZnS:Cu power was identified using X-ray diffraction (D8- Advanced, Bruker). Raman spectra of SWCNTs were collected by a Micro-Raman spectrometer (LabRAM HR Evolution, Horiba JY). The electrical characteristics of TENG, including output voltage and short-circuit current were measured by a Keithley Model 6514 high-impedance electrometer. The EL spectra were obtained through a compact spectrometer (NOVA, Ideaoptics). The capacitances of the polymer matrix were recorded on an Agilent E4980A Precision LCR meter at 1 kHz with custom LabVIEW programs. The relative permittivity (ε_r) of polymer matrix is determined by the following equation:

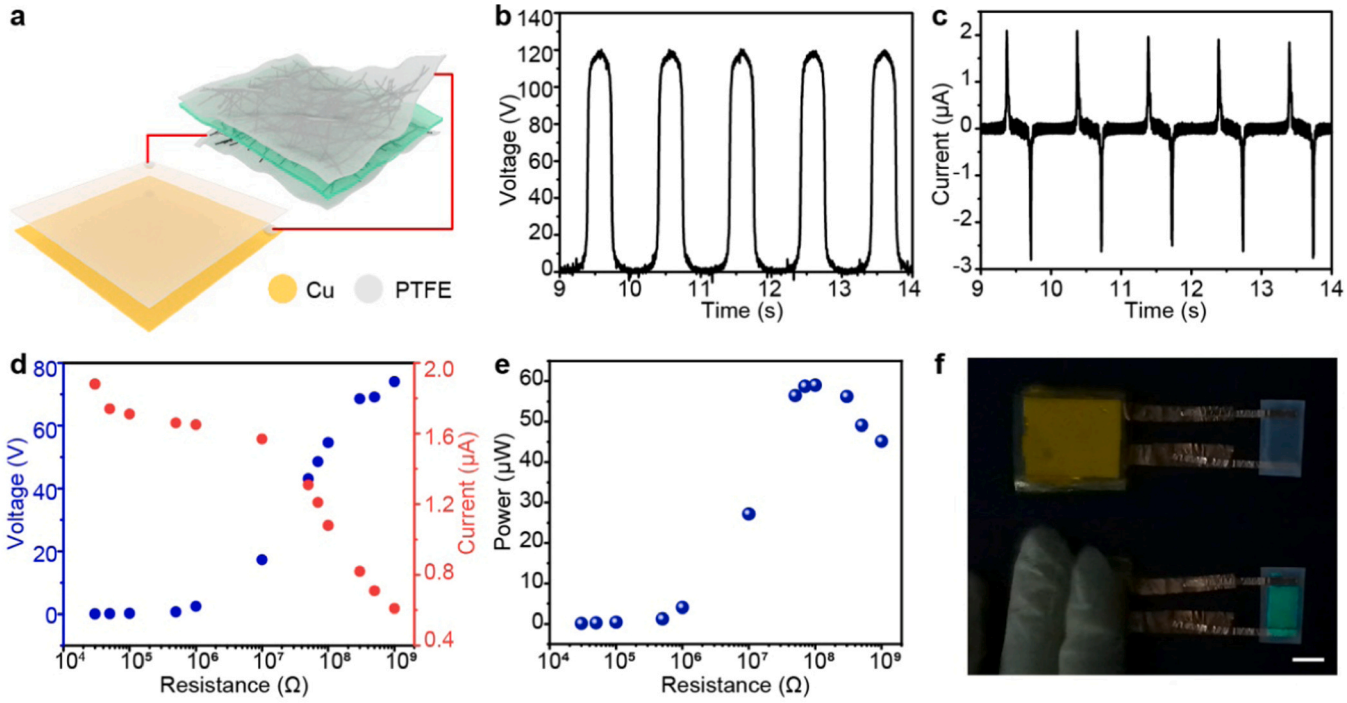

Fig. 2. Demonstration of self-powered ACEL devices. (a) Concept illustration of self-powered ACEL device. (b and c) Open circuit voltage and short circuit current of the TENG. (d and e) Output voltage, current, and power of the TENG under various load resistance. (f) Photograph of self-powered ACEL device. Scale bar: 1 cm.

$$\varepsilon_r = \frac{Cd}{\varepsilon_0 S}$$

where C is the capacitance, ε_0 is the vacuum permittivity (8.854×10^{-12} F m^{-1}), d is the thickness of the polymer matrix (120 μm), S is the area of electrode covering the polymer matrix.

3. Results and discussions

The ACEL device consists of three stacked components: two transparent electrodes and one emission layer, as shown in Fig. 1a. The SWCNT film is utilized to construct the electrodes on PDMS. The emission layer is prepared by blending ZnS:Cu powders in PDMS matrix. Therefore, the ACEL devices in this work are intrinsically excellent transparent and stretchable. The detailed fabrication process of ACEL

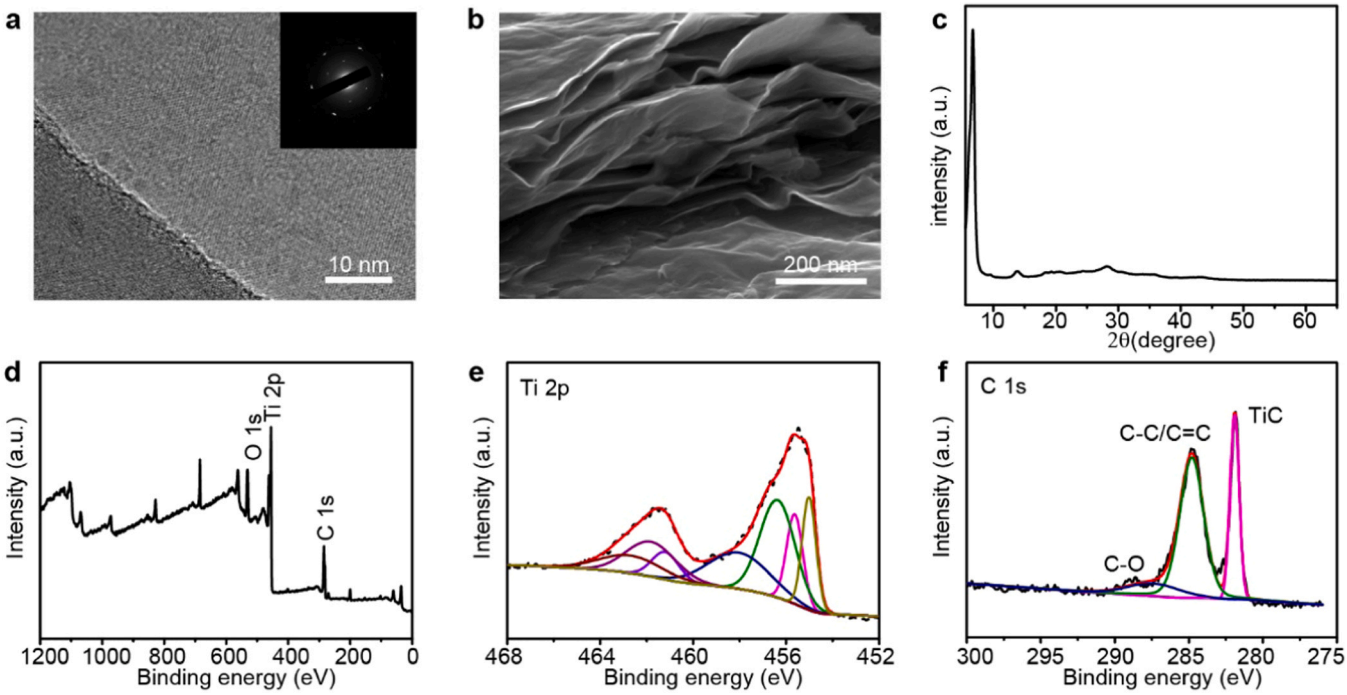

Fig. 3. Characterization of MXene. (a) TEM image and inset: SAED pattern of MXene Ti_3C_2 nanosheet. (b) Cross-section SEM image of MXene Ti_3C_2 nanosheets. (c) X-ray diffraction pattern of MXene Ti_3C_2 nanosheets. (d–f) XPS spectra of MXene Ti_3C_2 nanosheets and the curve-fitting results of Ti 2p, and C 1s.

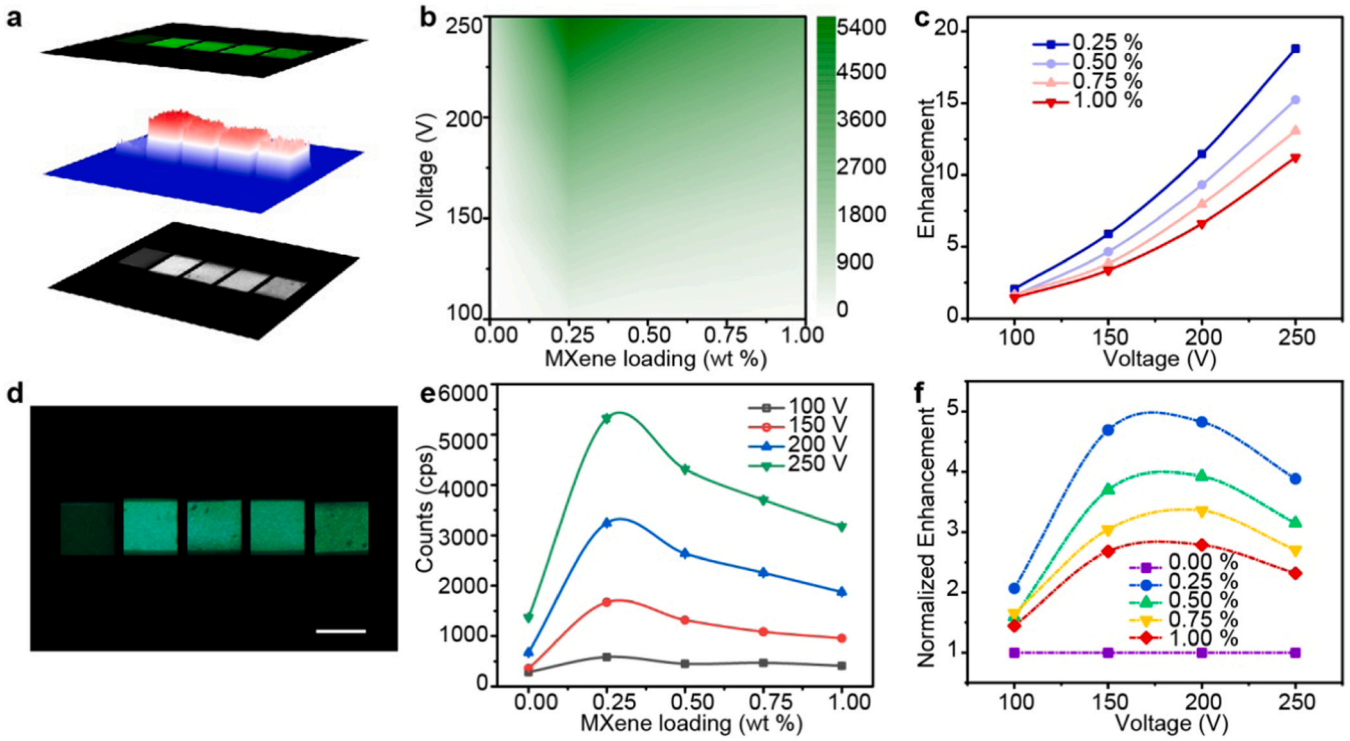

Fig. 4. Performance of ACEL devices with various MXene loadings. Electroluminescence intensities (a) and the corresponding optical images (d) of ACEL devices with various MXene loadings under 150 V. The EL intensities of ACEL devices with various MXene loadings under indifferent voltage (b, e) and the enhancement of ACEL devices compared with the one without MXene loading under 100 V (c) and the normalized enhancements of ACEL devices with various MXene loadings under the same voltages (f). Scale bar: 1 cm.

device is presented in Fig. S1. The ZnS:Cu powders are investigated by X-ray diffraction, photoluminescence (PL), and electroluminescence (EL). As shown in Fig. 1b, the diffraction peaks centered at 26.9°, 28.5°, and 30.5° are attributed to the scattering from the (1 0 0), (0 0 2) and (1 0 1) lattice surface of wurtzite ZnS (JCPDF # 36–1450), while those at 33.1° is from the lattice surface (200) of sphalerite phase (JCPDF # 05–0566). The PL and EL spectra of ZnS:Cu are presented in Fig. 1c. The emission at 502 nm arises from the shallowly trapped electrons to the t_2 level of Cu^{2+}[42]. The Raman spectra of the SWCNTs are shown in Fig. 1d. The characteristic Raman peaks at 185 cm^{-1} and 1585 cm^{-1} are attributed to the radial breathing mode (RBM) and the tangential mode (G band), respectively [41,43]. The performance of ACEL device powered under various voltages is demonstrated in Figs. 1e and f. The brightness of ACEL devices increase along with the voltage. And the corresponding optical images are illustrated in the inset of Fig. 1f.

As a vital part of self-power ACEL system, the TENG consisting of Cu and PTDE is illustrated in Fig. 2a. The output performance of the simple TENG is investigated and shown in Fig. 2b and c. The highest output voltage could reach 120 V, and the maximum short current is about 2 μA. The peak output power of TENG is about 60 μW with the load resistance of 10^8 Ω (Fig. 2e). This contact-mode TENG could easily power the ACEL device, as shown in Fig. 2f. When pressing the TENG, the ACEL device was lighted up. The detailed operation process of the self-powered ACEL system is shown in supporting movie S1.

Supplementary material related to this article can be found online at doi:10.1016/j.nanoen.2021.106077.

To enhance the performance of the self-powered ACEL system, a novel approach is utilized through decreasing the driving voltage of ACEL device. As is known, ACEL devices need to be driven at high-electric field intensity. And the emission powers (E_P) could be depicted with the following equation [44]:

$$E_P = \varepsilon_M V/(\varepsilon_M L_M + \varepsilon_P L_P)$$

where ε_M and ε_P are the relative permittivity of polymer matrix and phosphors, respectively; while L_M and L_P are the thickness of polymer matrix and phosphors. Therefore, the threshold driving voltage could be decreased through increasing the relative permittivity of polymer matrix.

MXene as a new class of 2D materials have been broadly studied in electrochemical and thermoelectric applications, and have been demonstrated to improve the relative permittivity of polymer matrix. Here, we utilize MXene to enhance the self-powered ACEL device. As shown in Fig. 3, the structure, morphology, and chemical composition of MXene are investigated by TEM, SEM, XRD, and XPS. The TEM image and selected area electron diffraction (SAED) patterns in Fig. 3a depicts the typical morphology of MXene nanosheet and high degree of crystallinity. The cross-section SEM image of the layered structure of vacuum-filtrated MXene nanosheets is clearly shown in Fig. 3b. The XRD patterns of MXene nanosheet is presented in Fig. 3c, with a representative strong (002) peak at 6.7°, corresponding to the d-spacing of 1.3 nm. The surface chemistry of MXene nanosheets was investigated by XPS. The full XPS survey and high-resolution spectra of Ti 2p and C1s are shown in Fig. 3d–f. The C1s spectra are deconvoluted into three Gaussian peaks at 284.6, 287.6, and 281.9 eV, corresponding to the binding energy of C–C/C=C, C–O, and Ti–C, respectively.

The performance of ACEL devices with various MXene ratios (from 0.00% to 1.00%) are presented in Fig. 4. The corresponding optical image shown in Fig. 4d evidences an obvious enhancement in the brightness compared to the ACEL device without MXene under same driving voltage. To evaluate the enhancement, the brightness is illustrated using a 3D contour in Fig. 4a. The EL spectra and optical images of ACEL devices with various MXene loading ratio and driving voltage were also collected and illustrated in Figs. S2–S3. The EL intensities are extracted as a matrix versus the MXene loading ratio and driving voltage, as shown in Fig. 4b and e. Obviously, the ACEL device with 0.25 wt% MXene loading under 250 V delivers the best performance.

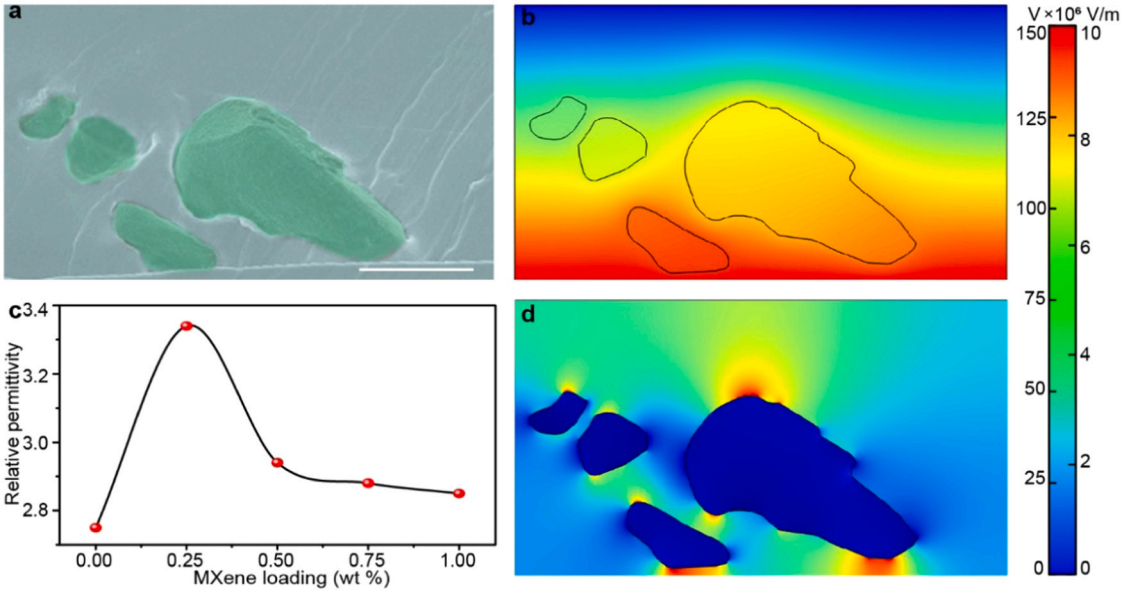

Fig. 5. Finite element simulation of ACEL devices under various MXene loadings. (a) Cross-section SEM image of ACEL device. Scale bar: 50 μm. (b, d) The simulated electric potential and field strength distribution of ACEL without MXene loading under 150 V. (c) The relative permittivity of PDMS matrix with various MXene loading.

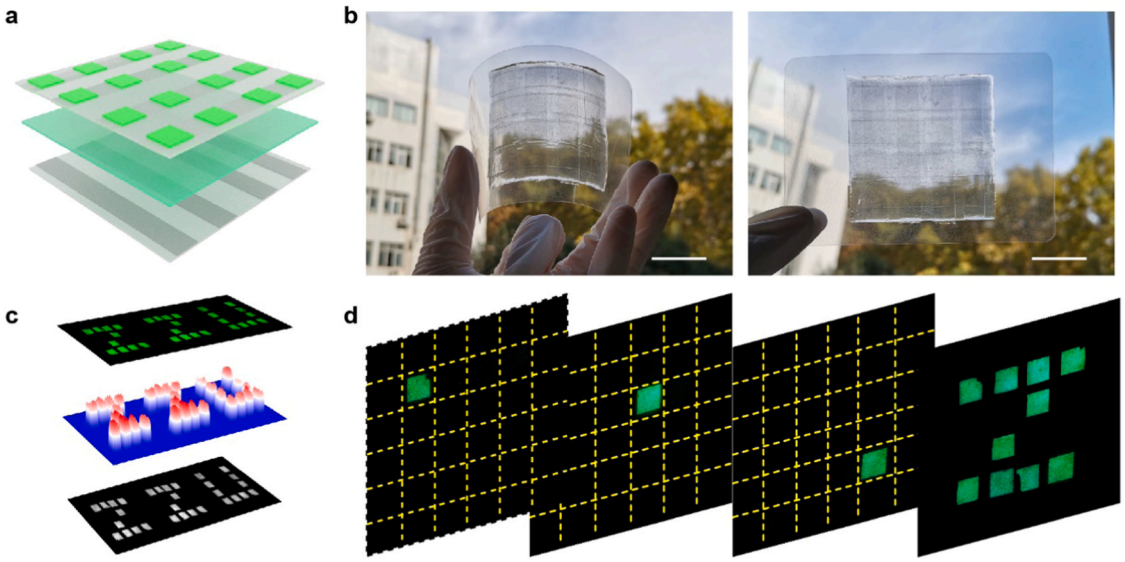

Fig. 6. Demonstration of transparent self-powered ACEL device array enhanced with MXene loading. (a and b) Schematic illustration and optical images of patterned ACEL device. (c) the EL intensity of AECL device with 'ZZU' pattern array. (d) the process of 'Z' pattern array. Scale bar: 2 cm.

The enhancements and normalized enhancements of EL intensities are shown in Fig. 4c and f. Compared with the original station that device without MXene loading under 100 V, the best enhancement reaches 2000% by the device with 0.25 wt% MXene loading under 250 V. The normalized enhancements were the enhancement of ACEL devices with various MXene loading under the same voltages. The best one possesses about 500% normalized enhancement.

In order to further understand the enhancement mechanism of ACEL via incorporating MXene in the PDMS matrix, a finite element analysis simulation (COMSOL Multiphysics) have been utilized to study the electric potential and field strength distribution. As shown in Fig. 5b and d, the simulated models of the same dimension are constructed according to the cross-section SEM image shown in Fig. 5a. The driving voltage for simulation is set as 100 V, and the relative permittivity of 9.6 and 2.75 for Zn:Cu powders and PDMS matrix are adopted, respectively. The electric potential and electric field intensity distribution depends on the morphologies and spatial distribution of Zn:Cu powders in PDMS matrix. The highest electric field intensity (10^7 V/m) is achieved at the protruding cape of ZnS:Cu powders. As an essential factor of ACEL device, the relative permittivity of the PDMS matrix with various MXene loadings are measured and shown in Fig. 5c. The detailed capacitances and relative permittivity are collected in Fig. S4 and Table S1. The relative permittivity increases with the MXene loading (from 0 to 0.25 wt%); further increase in the MXene loading leads to a drop in relative permittivity, indicating a percolation limit for the maximum MXene loading ratio [39]. The corresponding electric field distributions of ACEL with various relative permittivity are simulated and demonstrated in the movie S2.

Supplementary material related to this article can be found online at doi:10.1016/j.nanoen.2021.106077.

For practical applications, the patterned self-powered ACEL device with MXene loading is obtained and demonstrated. As illustrated in Fig. 6a, the patterned ACEL consists of the two crossed strip electrodes and an emission layer. The excellent flexibility and transparency of patterned ACEL device are evidenced in Fig. 6b. The transmittances of ACEL device with various MXene loadings are provided in Fig. S5. For the patterned self-powered ACELs with MXene loading, each pattern is powered and lighted up by a simple TENG, the corresponding optical images are recorded and illustrated in Figs. S6 and 6d. The pattern of 'ZZU' registered by the ACEL is illustrated in Fig. 6c. Each pixel of the pattern conveys the similar brightness, which is beneficial for developing self-powered ACEL displays and illumination for future applications in human–machine interactions, artificial electronic skins, and wearable equipment. In this work, the patterned display array is 4×4 pixels. And the dimensions each pixel is 4×4 mm^2. The resolution of the self-powered ACEL device array could be further improved by lithography to obtain patterned SWCNTs electrodes and patterned emissive layer [45,46].

4. Conclusion

MXene-enhanced self-powered ACEL devices have been fabricated for patterned displays. By introducing 0.25 wt% of MXene into the PDMS matrix, the EL intensity of the ACEL device can be enhanced by 500% while retains excellent transparency. The fundamental enhancing mechanism is elaborated by the finite element analysis. The ACEL device could be powered by TENG for patterned displays and illumination, which will expand a novel approach to self-powered communication in IoT.

CRediT authorship contribution statement

Junlu Sun: Conceptualization, Methodology, Formal analysis, Investigation, Visualization, Writing - original draft. **Yu Chang**: Methodology, Investigation, Visualization, Writing - original draft. **Lin Dong**: Conceptualization, Supervision, Writing - review & editing, Funding acquisition. **Kuikui Zhang**: Resources. **Qilin Hua**: Methodology, Investigation. **Jinhao Zang**: Methodology. **Qiushuo Chen**: Methodology. **Yuanyuan Shang**: Resources. **Caofeng Pan**: Conceptualization, Supervision, Writing - review & editing, Funding acquisition. **Chongxin Shan**: Conceptualization, Supervision, Writing - review & editing, Funding acquisition.

Declaration of Competing Interest

The authors declare that they have no known competing financial interests or personal relationships that could have appeared to influence the work reported in this paper.

Acknowledgments

The authors thank for the support of the National Natural Science Foundation of China (11674290, U1704138, 11974317 and 61904012), Shenzhen Science and Technology Program (Grant No. KQTD20170810105439418), and the Physics Discipline Improvement Program of Zhengzhou University.

Appendix A. Supporting information

Supplementary data associated with this article can be found in the online version at doi:10.1016/j.nanoen.2021.106077.

References

[1] D. Son, J. Kang, O. Vardoulis, Y. Kim, N. Matsuhisa, J.Y. Oh, J.W.F. To, J. Mun, T. Katsumata, Y. Liu, A.F. McGuire, M. Krason, F. Molina-Lopez, J. Ham, U. Kraft, Y. Lee, Y. Yun, J.B.H. Tok, Z. Bao, An integrated self-healable electronic skin system fabricated via dynamic reconstruction of a nanostructured conducting network, Nat. Nanotechnol. 13 (2018) 1057–1065.
[2] T. Yokota, P. Zalar, M. Kaltenbrunner, H. Jinno, N. Matsuhisa, H. Kitanosako, Y. Tachibana, W. Yukita, M. Koizumi, T. Someya, Ultraflexible organic photonic skin, Sci. Adv. 2 (2016), 1501856.
[3] Q. Hua, J. Sun, H. Liu, R. Bao, R. Yu, J. Zhai, C. Pan, Z.L. Wang, Skin-inspired highly stretchable and conformable matrix networks for multifunctional sensing, Nat. Commun. 9 (2018) 244.
[4] G. Chen, Y. Luo, H.Y. Gao, J. Jiang, Y.J. Yu, L. Zhang, Y. Zhang, X.G. Li, Z.Y. Zhang, Z.C. Dong, Phys. Rev. Lett. 122 (2019).
[5] Q. Shan, C. Wei, Y. Jiang, J. Song, Y. Zou, L. Xu, T. Fang, T. Wang, Y. Dong, J. Liu, B. Han, F. Zhang, J. Chen, Y. Wang, H. Zeng, Perovskite light-emitting/detecting bifunctional fibres for wearable LiFi communication, Light: Sci. Appl. 9 (2020) 163.
[6] H. Bai, S. Li, J. Barreiros, Y. Tu, C.R. Pollock, R.F. Shepherd, Stretchable distributed fiber-optic sensors, Science 370 (2020) 848–852.
[7] Y. Zhang, Z. Huo, X. Wang, X. Han, W. Wu, B. Wan, H. Wang, J. Zhai, J. Tao, C. Pan, Z.L. Wang, High precision epidermal radio frequency antenna via nanofiber network for wireless stretchable multifunction electronics, Nat. Commun. 11 (2020) 5629.
[8] C.-L. Shen, Q. Lou, C.-F. Lv, J.-H. Zang, S.-N. Qu, L. Dong, C.-X. Shan, Bright and multicolor chemiluminescent carbon nanodots for advanced information encryption, Adv. Sci. 6 (2019), 1802331.
[9] B. Lee, J.-Y. Oh, H. Cho, C.W. Joo, H. Yoon, S. Jeong, E. Oh, J. Byun, H. Kim, S. Lee, J. Seo, C.W. Park, S. Choi, N.-M. Park, S.-Y. Kang, C.-S. Hwang, S.-D. Ahn, J.-I. Lee, Y. Hong, Ultraflexible and transparent electroluminescent skin for real-time and super-resolution imaging of pressure distribution, Nat. Commun. 11 (2020) 663.
[10] T. Sekitani, H. Nakajima, H. Maeda, T. Fukushima, T. Aida, K. Hata, T. Someya, Stretchable active-matrix organic light-emitting diode display using printable elastic conductors, Nat. Mater. 8 (2009) 494–499.
[11] M.S. White, M. Kaltenbrunner, E.D. Głowacki, K. Gutnichenko, G. Kettlgruber, I. Graz, S. Aazou, C. Ulbricht, D.A.M. Egbe, M.C. Miron, Z. Major, M.C. Scharber, T. Sekitani, T. Someya, S. Bauer, N.S. Sariciftci, Ultrathin, highly flexible and stretchable PLEDs, Nat. Photonics 7 (2013) 811–816.
[12] J. Liang, L. Li, X. Niu, Z. Yu, Q. Pei, Elastomeric polymer light-emitting devices and displays, Nat. Photonics 7 (2013) 817–824.
[13] R.R. Bao, C.F. Wang, L. Dong, C.Y. Shen, K. Zhao, C.F. Pan, CdS nanorods/organic hybrid LED array and the piezo-phototronic effect of the device for pressure mapping, Nanoscale 8 (2016) 8078–8082.
[14] J. Song, J. Li, X. Li, L. Xu, Y. Dong, H. Zeng, Quantum dot light-emitting diodes based on inorganic perovskite cesium lead halides ($CsPbX_3$), Adv. Mater. 27 (2015) 7162–7167.
[15] X. Li, Y. Wu, S. Zhang, B. Cai, Y. Gu, J. Song, H. Zeng, $CsPbX_3$ quantum dots for lighting and displays: room-temperature synthesis, photoluminescence superiorities, underlying origins and white light-emitting diodes, Adv. Funct. Mater. 26 (2016) 2435–2445.
[16] H.B. Shen, Q. Gao, Y.B. Zhang, Y. Lin, Q.L. Lin, Z.H. Li, L. Chen, Z.P. Zeng, X.G. Li, Y. Jia, S.J. Wang, Z.L. Du, L.S. Li, Z.Y. Zhang, Fabrication and evaluation a transferrin receptor targeting nano-drug carrier for cerebral infarction treatment, Artif. Cells, Nanomed., Biotechnol. 47 (2019) 192–200.
[17] R. Bao, C. Wang, L. Dong, R. Yu, K. Zhao, Z.L. Wang, C. Pan, Flexible and controllable piezo-phototronic pressure mapping sensor matrix by ZnO NW/p-polymer LED array, Adv. Funct. Mater. 25 (2015) 2884–2891.
[18] Y.-J. Lu, Z.-F. Shi, C.-X. Shan, D.-Z. Shen, ZnO-based deep-ultraviolet light-emitting devices, Chin. Phys. B 26 (2017), 047703.
[19] C. Pan, L. Dong, G. Zhu, S. Niu, R. Yu, Q. Yang, Y. Liu, Z.L. Wang, High-resolution electroluminescent imaging of pressure distribution using a piezoelectric nanowire LED array, Nat. Photonics 7 (2013) 752–758.
[20] B.T. Howard, H.F. Ivey, W. Lehmann, Voltage dependence of electroluminescent brightness, Phys. Rev. 96 (1954) 799–800.
[21] W.W. Piper, F.E. Williams, Theory of electroluminescence, Phys. Rev. 98 (1955) 1809–1813.
[22] H. Fang, H. Tian, J. Li, Q. Li, J. Dai, T.-L. Ren, G. Dong, Q. Yan, Self-powered flat panel displays enabled by motion-driven alternating current electroluminescence, Nano Energy 20 (2016) 48–56.
[23] X. Wang, J. Sun, L. Dong, C. Lv, K. Zhang, Y. Shang, T. Yang, J. Wang, C.-X. Shan, Stretchable and transparent electroluminescent device driven by triboelectric nanogenerator, Nano Energy 58 (2019) 410–418.
[24] Z.L. Wang, Triboelectric nanogenerators as new energy technology for self-powered systems and as active mechanical and chemical sensors, ACS Nano 7 (2013) 9533–9557.
[25] F.-R. Fan, Z.-Q. Tian, Z. Lin, Wang, Flexible triboelectric generator, Nano Energy 1 (2012) 328–334.
[26] P. Chen, J. An, S. Shu, R. Cheng, J. Nie, T. Jiang, Z.L. Wang, Super-durable, low-wear, and high-performance fur-brush triboelectric nanogenerator for wind and water energy harvesting for smart agriculture, Adv. Energy Mater. 11 (2021), 2003066.
[27] W. Xu, H. Zheng, Y. Liu, X. Zhou, C. Zhang, Y. Song, X. Deng, M. Leung, Z. Yang, R. X. Xu, Z.L. Wang, X.C. Zeng, Z. Wang, A droplet-based electricity generator with high instantaneous power density, Nature 578 (2020) 392–396.
[28] M. Zheng, S. Lin, Z. Tang, Y. Feng, Z.L. Wang, Photovoltaic effect and tribovoltaic effect at liquid-semiconductor interface, Nano Energy 83 (2021), 105810.
[29] X. Wang, H. Zhang, L. Dong, X. Han, W. Du, J. Zhai, C. Pan, Z.L. Wang, Self-powered high-resolution and pressure-sensitive triboelectric sensor matrix for real-time tactile mapping, Adv. Mater. 28 (2016) 2896–2903.

[30] L. Chen, C. Wen, S.-L. Zhang, Z.L. Wang, Z.-B. Zhang, Artificial tactile peripheral nervous system supported by self-powered transducers, Nano Energy 82 (2021), 105680.
[31] J. Du, J. Duan, X. Yang, Y. Wang, Y. Duan, Q. Tang, Charge boosting and storage by tailoring rhombus all-inorganic perovskite nanoarrays for robust triboelectric nanogenerators, Nano Energy 74 (2020), 104845.
[32] Y. Wang, X. Yang, X. Yu, J. Duan, Q. Yang, Y. Duan, Q. Tang, Triboelectric charging behaviors and photoinduced enhancement of alkaline earth ions doped inorganic perovskite triboelectric nanogenerators, Nano Energy 77 (2020), 105280.
[33] Z.L. Wang, T. Jiang, L. Xu, Toward the blue energy dream by triboelectric nanogenerator networks, Nano Energy 39 (2017) 9–23.
[34] H. Zhao, X. Xiao, P. Xu, T. Zhao, L. Song, X. Pan, J. Mi, M. Xu, Z.L. Wang, Dual-tube helmholtz resonator-based triboelectric nanogenerator for highly efficient harvesting of acoustic energy, Adv. Energy Mater. 9 (2019), 1902824.
[35] S.Y. Lu, L.Z. Sui, Y. Liu, X. Yong, G.J. Xiao, K.J. Yuan, Z.Y. Liu, B.Z. Liu, B. Zou, B. Yang, White photoluminescent Ti_3C_2 MXene quantum dots with two-photon fluorescence, Adv. Sci. 6 (2019), 1801470.
[36] M. Naguib, V.N. Mochalin, M.W. Barsoum, Y. Gogotsi, 25th anniversary article: MXenes: a new family of two-dimensional materials, Adv. Mater. 26 (2014) 992–1005.
[37] T.K. Zhao, P.F. Zhai, Z.H. Yang, J.X. Wang, L.B. Qu, F.G. Du, J.T. Wang, Self-supporting Ti_3C_2Tx foam/S cathodes with high sulfur loading for high-energy-density lithium-sulfur batteries, Nanoscale 10 (2018) 22954–22962.
[38] L. Wei, J.-W. Wang, X.-H. Gao, H.-Q. Wang, X.-Z. Wang, H. Ren, Enhanced dielectric properties of a poly(dimethyl siloxane) bimodal network percolative composite with MXene, ACS Appl. Mater. Interfaces 12 (2020) 16805–16814.
[39] S. Tu, Q. Jiang, X. Zhang, H.N. Alshareef, Large dielectric constant enhancement in MXene percolative polymer composites, ACS Nano 12 (2018) 3369–3377.
[40] S. Tu, Q. Jiang, J. Zhang, X. He, M.N. Hedhili, X. Zhang, H.N. Alshareef, Enhancement of dielectric permittivity of $Ti_3C_2T_x$ MXene/polymer composites by controlling flake size and surface termination, ACS Appl. Mater. Interfaces 11 (2019) 27358–27362.
[41] Y. Shang, C. Hua, W. Xu, X. Hu, Y. Wang, Y. Zhou, Y. Zhang, X. Li, A. Cao, Meter-long spiral carbon nanotube fibers show ultrauniformity and flexibility, Nano Lett. 16 (2016) 1768–1775.
[42] Y. Deng, J. Wei, J. Sun, Y. Zhang, L. Dong, C.-X. Shan, Enhancing the mechanoluminescence of traditional ZnS:Mn phosphors via Li^+ Co-doping, J. Lumin. 225 (2020), 117364.
[43] Y. Shang, C. Wang, X. He, J. Li, Q. Peng, E. Shi, R. Wang, S. Du, A. Cao, Y. Li, Self-stretchable, helical carbon nanotube yarn supercapacitors with stable performance under extreme deformation conditions, Nano Energy 12 (2015) 401–409.
[44] P.D. Rack, A. Naman, P.H. Holloway, S.S. Sun, R.T. Tuenge, Materials used in electroluminescent displays, MRS Bull. 21 (2013) 49–58.
[45] L. Xiang, H. Zhang, G. Dong, D. Zhong, J. Han, X. Liang, Z. Zhang, L.-M. Peng, Y. Hu, Low-power carbon nanotube-based integrated circuits that can be transferred to biological surfaces, Nat. Electron. 1 (2018) 237–245.
[46] P. Jothimuthu, A. Carroll, A.A.S. Bhagat, G. Lin, J.E. Mark, I. Papautsky, Photodefinable PDMS thin films for microfabrication applications, J. Micromech. Microeng. 19 (2009), 045024.

Junlu Sun received his master's degree in Materials Science & Engineering from Zhengzhou University in 2014. He is currently a PhD Candidate majored in Optics at Zhengzhou University. He has joined in the group of Professor Caofeng Pan at Beijing Institute of Nanoenergy and Nanosystems, CAS as a visiting student since 2015. His research focuses on flexible stretchable optoelectronics and self-powered display system.

Yu Chang received her Bachelor's degree in Xinzhou Normal University in 2019. She is currently a postgraduate student in the School of Physics & Microelectronics, Zhengzhou University. Her research focuses on flexible multifunctional electroluminescence devices.

Prof. Lin Dong received his B.S. (1998) and M.S. degree (2001) in Chemistry from Jilin University, and the PhD degree (2005) in Condensed Matter Physics from Changchun Institute of Optics, Fine Mechanics and Physics, CAS. He joined Zhengzhou University in 2005. He is currently a professor in School of Physics & Microelectronics, Zhengzhou University. His research interest is mainly focused on mechanoluminescence and piezotronic/piezophototronic derived nanomaterials and devices.

Kuikui Zhang received his Bachelor's degree in Jiangxi Science and Technology Normal University in 2016. Now he is pursuing his doctor's degree in Zhengzhou University. His research interest focuses on the synthesis of nanoparticles and their biological application.

Qilin Hua received his PhD degree in microelectronics from University of Chinese Academy of Sciences in 2016. He then joined Tsinghua University. He is currently an associate professor at Beijing Institute of Nanoenergy and Nanosystems, CAS. His research interests include flexible/stretchable electronics, lowdimensional materials, GaN-based devices, memristors, and neuromorphic systems.

Jinhao Zang received his MS degree from Northwest University in 2008. He is currently a staff scientist in School of Physics & Microelectronics, Zhengzhou University. His research focuses on high pressure synthesis of novel materials.

Qiushuo Chen received his master's degree in condensed matter physics from College of Physics and Electronic Engineering, Chongqing Normal University in 2020. Since 2018, he has joined in the group of Professor Caofeng Pan at Beijing Institute of Nanoenergy and Nanosystems, CAS as a visiting student being educated. His research focuses on piezoelectronics and piezoelectric optoelectronics.

Yuanyuan Shang received both her B.A. (2007) and PhD (2015) in Materials Science at Harbin Institute of Technology. Currently, she is working at Zhengzhou University. Her research focuses on the development of carbon nanotube and composite fibers for flexible devices.

Prof. Caofeng Pan received his B.S. degree (2005) and PhD degree (2010) in Materials Science and Engineering from the Tsinghua University, China. He then joined the group of Prof. Zhong Lin Wang at the Georgia Institute of Technology as a postdoctoral fellow from 2010 to 2013. He is currently a professor and a group leader at the Beijing Institute of Nanoenergy and Nanosystems, CAS. His research interests mainly focus on piezotronics/piezophototronics for new electronic and optoelectronic devices, nanopower source, hybrid nanogenerators, and selfpowered nanosystems.

Prof. Chong-Xin Shan obtained his BS degree from Wuhan University in 1999, and PhD degree from Changchun Institute of Optics, Fine Mechanics and Physics (CIOMP), CAS in 2004. Then he worked in sequence in Chinese University of Hong Kong and University of Nottingham as a postdoctoral researcher, and returned to CIOMP as "Hundred Talent" professor in 2008. He moved to Zhengzhou University in 2015, and is currently the Dean of School of Physics. His research interest is mainly focused on wide band gap semiconductor materials and optoelectronic devices.